Photodissociation of 1-bromo-2-butene, 4-bromo-1-butene, and cyclopropylmethyl bromide at 234 nm studied using velocity map imaging

Kai-Chung Lau, Yi Liu, and Laurie J. Butler[a)]
James Franck Institute and Department of Chemistry, The University of Chicago, Chicago, Illinois 60637

(Received 21 July 2006; accepted 17 August 2006; published online 11 October 2006)

We present photofragment imaging experiments to characterize potential photolytic precursors of three C_4H_7 radical isomers: 1-methylallyl, cyclopropylmethyl, and 3-buten-1-yl radicals. The experiments use 2+1 resonance enhanced multiphoton ionization (REMPI) with velocity map imaging to state-selectively detect the $Br(^2P_{3/2})$ and $Br(^2P_{1/2})$ atoms as a function of their recoil velocity imparted upon photodissociation of 1-bromo-2-butene, cyclopropylmethyl bromide, and 4-bromo-1-butene at 234 nm as well as the angular distributions of the photofragments. Energy and momentum conservation allows the internal energy distribution of the nascent momentum-matched radicals to be derived. The radicals are detected with single photon photoionization at 157 nm. In the case of the 1-methylallyl radical the photoionization cross section is expected to be independent of internal energy in the range of 7–30 kcal/mol. Thus, comparison of the product recoil kinetic energy distribution derived from the measurement of the 1-methylallyl velocity distribution, detecting the radicals with 157 nm photoionization, with a linear combination of the Br atom recoil kinetic energy distributions allows us to derive reliable REMPI line strength ratios for the detection of Br atoms and to test the assumption that the photoionization cross section does not strongly depend on the internal energy of the radical. This line strength ratio is then used to determine the branching to the $Br(^2P_{3/2})$ and $Br(^2P_{1/2})$ product channels for the other two photolytic systems and to determine the internal energy distribution of their momentum-matched radicals. (We also revisit earlier work on the photodissociation of cyclobutyl bromide which detected the Br atoms and momentum-matched cyclobutyl radicals.) This allows us to test whether the 157 nm photoionization of these radicals is insensitive to internal energy for the distribution of total internal (vibrational +rotational) energy produced. We find that 157 nm photoionization of cyclopropylmethyl radicals is relatively insensitive to internal energy, while 3-buten-1-yl radicals show a photoionization cross section that is markedly dependent on internal energy with the lowest internal energy radicals not efficiently detected by photoionization at 157 nm. We present electronic structure calculations of the radicals and their cations to understand the experimental results. © *2006 American Institute of Physics*. [DOI: 10.1063/1.2353836]

I. INTRODUCTION

This paper investigates several brominated hydrocarbons as potential photolytic precursors for the generation of hydrocarbon radicals. Compared with the chlorohydrocarbons, the primary photodissociation of bromohydrocarbons at 234 nm can be more straightforward; C–Br fission often dominates, with significantly less contribution from hydrogen halide elimination. Furthermore, this work suggests that C–Br fission at 234 nm results in only ground electronic state radicals from these precursors, whereas halogenated photolytic precursors of other radicals have produced some fraction of the radicals in an excited electronic state when photodissociated at 193 nm.[1–4] This is an advantage if one wishes to study the excited states of the radical,[5] but can complicate studies which use the precursor in spectroscopically based kinetics experiments[6] on radical reactions or energy transfer. For a given alkyl or alkenyl bromide, if the Br atom spin-orbit states can be state-selectively detected, along with simultaneous measurement of the kinetic energy release distribution, the internal energy distribution of the recoiling hydrocarbon radicals can be accurately determined. This paper thus also presents the internal energy distribution of the nascent radicals.

There have been a number of studies on the uv photodissociation of alkyl and alkenyl bromides in the literature.[1,7–10] Gougousi *et al.*[7] extensively investigated the photolysis of methyl bromide in the first continuum, resolving the $Br(^2P_{3/2})/Br(^2P_{1/2})$ spin-orbit branching ratio, the partial absorption cross section, as well as the vibrational distribution of the nascent CH_3 radicals. Park *et al.*[10] studied the 235 nm photodissociation dynamics of allyl bromide, and found a single-peaked product translational energy release distribution $[P(E_T)]$, unlike that of the allyl chloride $P(E_T)$. A series of *n*-alkyl bromides was studied at 234 and 267 nm by Zhu *et al.*;[8] the study determined the relative quantum yields of the $Br(^2P_{3/2})$ and $Br(^2P_{1/2})$ fragments and rationalized the observed trends. Morton *et al.*[9] and Miller *et al.*[1]

[a)]Electronic mail: l-butler@uchicago.edu

investigated the 193 nm photodissociation of 1-bromopropene and 2-bromo-1-butene, respectively, using tunable vacuum ultraviolet (vuv) photoionization of the photofragments.

Very recently, we have studied the C–Br bond fission of cyclobutyl bromide (c-C_4H_7Br) at 234 nm using the velocity map imaging method. We have state selectively detected the $Br(^2P_{3/2})$ and $Br(^2P_{1/2})$ atomic fragments by resonance enhanced multiphoton ionization (REMPI) at 234 nm and the momentum-matched cyclobutyl (c-C_4H_7) radical by 157 nm single photon ionization. By comparing the total translational energy release distribution derived from the measured recoil velocities of the Br atoms with that derived from the momentum-matched c-C_4H_7 radical cophotofragments, we have determined the spin-orbit branching ratio for $Br(^2P_{1/2})$ to $Br(^2P_{3/2})$ channels as well as the relative REMPI line strength ratio for $Br(^2P_{1/2})$ and $Br(^2P_{3/2})$ at the corresponding wavelengths. The c-C_4H_7 radicals generated in the 234 nm photodissociation are found to have an internal energy range of 10–35 kcal/mol. The determination of the spin-orbit branching ratio (and the REMPI line strength factor) was based on the assumption that the photoionization probability of the cyclobutyl radical at 157 nm is uniform over the internal energy range in which the radical is generated. Here we test the validity of this assumption for three other C_4H_7 radical species. Note also that the prior work on the c-C_4H_7 radical precursor evidenced only a small branching to the $Br(^2P_{1/2})$ channel, so the quality of the overall fit did not depend sensitively on the fraction of the $Br(^2P_{1/2})$ channel included. Thus the derived REMPI line strength factor was given with large error bars. In addition, the assumption that the photoionization of the c-C_4H_7 radical was independent of internal energy over the range of internal energies probed may only roughly hold as the c-C_4H_7 radical could ionize into at least three possible c-C_4H_7 cationic structures at the photon energy of 7.9 eV. The ionization threshold in forming these three c-C_4H_7 cationic structures ranges from 7.0 to 7.6 eV. One may expect that the photoionization process in yielding a cationic structure similar to its initial neutral structure should be more favorable than that in yielding a cationic structure significantly different from the initial neutral structure. This is because the Franck-Condon overlap between the vibrational envelope of the neutral and that of the cation is larger. Thus, the relative REMPI line strength factor for $Br(^2P_{1/2})$ and $Br(^2P_{3/2})$ deduced by comparing the $P(E_T)$'s between the momentum-matched Br and the c-C_4H_7 cofragments (generated in the C–Br bond fission of cyclobutyl bromide) may not be reliable enough because of the presence of multiple photoionization channels with different photoionization probabilities for the c-C_4H_7 fragments.

To further investigate the validity of the spin-orbit branching ratio (and the REMPI line strength) in our previous photodissociation experiment and to explore the photodissociation dynamics of other C_4H_7Br molecules, we present here our new photodissociation studies on 1-bromo-2-butene ($CH_2BrCH{=}CHCH_3$), cyclopropylmethyl bromide (c-$CH_2Br{-}CHCH_2CH_2$), and 4-bromo-1-butene ($CH_2{=}CHCH_2CH_2Br$) using our velocity map imaging apparatus. In particular, we chose 1-bromo-2-butene because it generates the 1-methylallyl radical ($CH_2CH{=}CHCH_3$) with an internal energy ranged below its dissociation and isomerization barriers at 234 nm. The 1-methylallyl radicals thus produced in the C–Br bond fission of 1-bromo-2-butene are thermodynamically stable and ionize solely into the 1-methylallyl cations, which is also a local minimum (with a deep well) on the potential energy surface of $C_4H_7^+$. Thus we expect the photoionization probability of the 1-methylallyl radicals to be uniform over the internal energies produced. The $Br(^2P_{1/2})/Br(^2P_{3/2})$ product branching derived from the momentum-matched Br fragments and 1-methylallyl radicals is then likely to be more accurate and the data analysis gives a reliable REMPI line strength factor for detection of Br atoms in these spin-orbit states.

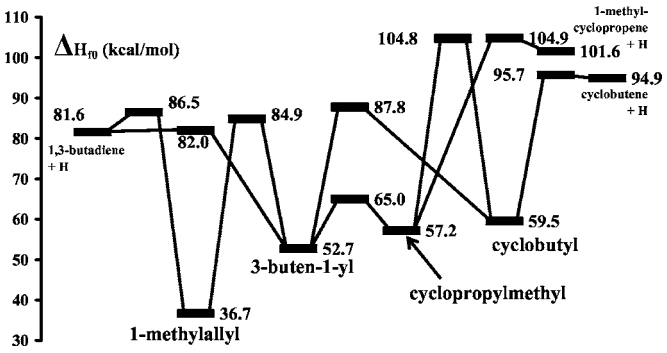

FIG. 1. Potential energy surface displaying the dissociation and isomerization channels among the 1-methylallyl, cyclopropylmethyl, 3-buten-1-yl, and cyclobutyl radicals. The $\Delta H_{f0\ K}$ values are obtained at the G3//B3LYP level. Note that the ring-opening barrier between cyclobutyl and 3-buten-1-yl radicals was misconnected between cyclobutyl and cyclopropylmethyl radicals in our previous study (Fig. 5 in Ref. 14). The methylene shift barrier between cyclobutyl and cyclopropylmethyl radicals has now been located and included here.

The other two studies reported here, the 234 nm photodissociation of cyclopropylmethyl bromide to Br +cyclopropylmethyl radicals and the 234 nm photodissociation of 4-bromo-1-butene to Br+3-buten-1-yl radicals ($CH_2{=}CHCH_2CH_2$), investigate systems that are potentially more complicated. The cyclopropylmethyl radical produced in the photodissociation of cyclopropylmethyl bromide could be formed at high enough internal energies to be subjected to isomerization followed by H atom loss, as shown in Fig. 1. In the last system, the cation of the 3-buten-1-yl radical is unstable with respect to isomerization (there is no minimum on the cation potential surface with the radical center on the end carbon), so assuming that the photoionization cross section of this radical is independent of internal energy may not be valid. These experiments investigate that dependence.

These experiments measure both the angular and the velocity distributions of the nascent $Br(^2P_{3/2})$ and $Br(^2P_{1/2})$ atoms and the C_4H_7 cofragments. When the radical's photoionization cross section is independent of internal energy, we can deduce the spin-orbit branching ratio of Br atom fragments without prior knowledge of the REMPI line strength factor by comparing the total C–Br bond fission $P(E_T)$ obtained from the corresponding C_4H_7 radical photofragments with that from linear combinations of the $P(E_T)$'s derived

from the measured $Br(^2P_{3/2,1/2})$ products' velocity distributions. The best fit linear combination gives the branching fraction for producing Br atoms in each spin-orbit state. Then comparison of the relative Br atom REMPI signal levels gives the REMPI line strength factor needed to determine the product branching in other systems for which detecting the radical is more complicated. We use non-state-selective 157 nm photoionization in an attempt to detect all the C_4H_7 fragments formed in the 234 nm photodissociation with equal efficiency. The ionization energies (IEs) for all the C_4H_7 radicals generated by all three precursors are around 7.0–7.5 eV,[11] which is accessible by a 157 nm F_2 excimer laser. The atomic $Br(^2P_{3/2})$ and $Br(^2P_{1/2})$ fragments are probed by REMPI at 233.681 and 234.021 nm, respectively. This procedure works well, as expected, for the momentum-matched Br atoms and 1-methylallyl radicals, yielding both a branching ratio for production of the Br atom in each spin-orbit state and a reliable REMPI line strength factor. In contrast, the data on 1-bromo-4-butene indicate that there is a marked dependence of the photoionization cross section on the internal energy of the radical. On the basis of momentum and energy conservation, the $P(E_T)$ obtained from the kinetic energy release measurements of 3-buten-1-yl radical fragments would precisely match that of the atomic Br cofragments if none of the radicals underwent a dissociation and isomerization (see Fig. 1) and the photoionization cross section is independent of the internal energy of the radical for the population of nascent 3-buten-1-yl radicals, yet our data show that the radicals formed with lower internal energy are much less efficiently detected than higher internal energy radicals. Our associated electronic structure calculations attribute this to the prediction that the 3-buten-1-yl radicals are unstable upon ionization and convert readily to the 1-methylallyl cationic structure by a 2,1-hydrogen shift.

II. EXPERIMENT

The experimental two-dimensional photofragment velocity map ion imaging apparatus has been described in detail previously.[12–14] Samples of 1-bromo-2-butene, cyclopropylmethyl bromide, and 4-bromo-1-butene were purchased from Aldrich and used without further purification. The sample was introduced into the photodissociation region in the form of a seeded and skimmed supersonic beam. The liquid sample (10%) was bubbled through by helium (90%) prior to the expansion through a pulsed valve (nozzle diameter ≈0.6 mm) at a stagnation pressure of 500 Torr.

The 532 nm output of a Nd:YAG (yttrium aluminum garnet) continuum laser was used to pump a dye laser (Lambda Physik, FL3002, LDS698 dye) which generates visible radiation in the region of 675–715 nm. The dye laser output was frequency doubled in a potassium dihydrogen phosphate (KDP) crystal and the resulting 353 nm light was mixed with the 706 nm fundamental in a beta-barium borate (BBO) crystal to produce the 234 nm uv radiation. A focusing lens (focal length ≈109 mm) was used to focus the 234 nm laser into the chamber. The 234 nm light is linearly polarized along an axis vertically perpendicular to the molecular beam and parallel to the detector surface. The three respective C_4H_7Br precursors are dissociated by the 234 nm photons. The $Br(^2P_{3/2})$ and $Br(^2P_{1/2})$ fragments are ionized via 2+1 REMPI at 233.681 nm $(5p\ ^4P_{1/2} \leftarrow 4p\ ^2P_{3/2})$ and 234.021 nm $(5p\ ^2S_{1/2} \leftarrow 4p\ ^2P_{1/2})$, respectively. A 157 nm F_2 excimer laser (EX10F/300) is used to ionize the C_4H_7 radical fragments formed in the photodissociation of the precursor. The 157 nm laser is focused into the reaction chamber by a focusing lens (focal length ≈50 mm) and the light path is purged with nitrogen gas. During the experiment, the pulse energy (≈0.5 mJ per pulse) of the 234 laser beam was reduced substantially to minimize Coulomb repulsion between the ions formed in the photodissociation region.

The spherically expanding ion clouds formed in the photodissociation are accelerated toward a two-dimensional position-sensitive detector by an electrical ion lens assembly with a repeller/extractor voltage ratio of 1.404. After flying through the time-of-flight (TOF) drift region (≈577 mm), the ions were collected by a detector (Burle 3040FM) which consists of a chevron microchannel plate (MCP) coupled with a P20 phosphor screen by fiber optics. In order to detect only the ions of interest, the front plate of the MCP was pulsed to −750 V at the appropriate arrival time with a width of about 70 ns. The phosphor screen was maintained at 3.5 kV above the potential of the rear MCP plate. Images appearing on the phosphor screen were recorded by a 1376 × 1040 pixel charge-coupled device camera (LaVision Imager 3) with a standard 35 mm camera lens. The ion signal was obtained by using the event-counting algorithm in the DAVIS software and each image was accumulated for over 100 000 laser shots. The timing sequence for opening of the pulsed valve, firing of the Nd:YAG and F_2 excimer lasers, pulsing the MCP, and capturing the ion images were controlled by a digital pulse generator (Stanford Research DG535) at a repetition rate of 20 Hz. During the detection of the $Br(^2P_{1/2})$ and $Br(^2P_{3/2})$ fragments, the laser was scanned over the Doppler profile. The reconstruction of the images to three-dimensional scattering distributions was performed using the Gaussian basis-set expansion Abel transformation method developed by Dribinski *et al.*[15]

III. RESULTS AND ANALYSIS

This experiment investigates the following three photodissociation reactions:

$$CH_2BrCH{=}CHCH_3 \rightarrow CH_2CH{=}CHCH_3 + Br(^2P_{3/2,1/2}), \quad (1)$$

$$c\text{-}CH_2Br - CHCH_2CH_2 \rightarrow c\text{-}CH_2 - CHCH_2CH_2 + Br(^2P_{3/2,1/2}), \quad (2)$$

$$CH_2{=}CHCH_2CH_2Br \rightarrow CH_2{=}CHCH_2CH_2 + Br(^2P_{3/2,1/2}). \quad (3)$$

The bond dissociation energies (D_0) for the C–Br bond fission channels, reactions (1)–(3), calculated at the Gaussian-3 (G3//B3LYP) level of theory,[16,17] are displayed in Table I. Assuming effective rotational cooling in the supersonic expansion, the internal energies due to vibrational mo-

TABLE I. The bond dissociation energy [D_0(C–Br)], initial vibrational energy contents at 298 K, and available energy in kcal/mol after photodissociation for each individual C_4H_7Br precursor.

	D_0(C–Br)[a]	Vibrational contribution to E_{int} at 298 K	Energy available after 234 nm photodissociation[b]
trans-$CH_2BrCH{=}CHCH_3$	75.6	2.3	48.9
cis-$CH_2BrCH{=}CHCH_3$	75.3	2.2	49.1
c-$CH_2Br{-}CHCH_2CH_2$	68.2	1.8	55.8
trans-$CH_2{=}CHCH_2CH_2Br$	69.8	2.2	54.5
cis-$CH_2{=}CHCH_2CH_2Br$	69.2	2.1	55.1

[a]The *trans*-conformer of C_4H_7 radicals is more stable than the *cis*-conformer. The D_0(C–Br)'s are computed relative to the corresponding *trans*-radicals.
[b]Energy available is computed as photon energy (234 nm)+(vibrational contribution to E_{int})$-D_0$(C–Br).

tion for the corresponding parent molecules are also estimated using the 298 K vibrational frequencies calculated at the B3LYP/6-31G(*d*) level of theory and included in Table I. Thus, the energy available to partition between product recoil translational energy and internal energy of the nascent C_4H_7 radicals and bromine atom spin-orbit energy for reactions (1)–(3) are listed in Table I. There are two conformers (*cis* and *trans*) for the 1-bromo-2-butene and 4-bromo-1-butene precursors. The G3//B3LYP theory predicts that the relative stabilities of both conformers differ by 0.3–0.6 kcal/mol. Thus, both conformers are indistinguishable, given the experimental uncertainty in this study and the accuracy of the theoretical methods employed here. As the experiment is a one-color process while detecting the $Br(^2P_{1/2,3/2})$ fragments, the photodissociation wavelength varies slightly with the specific spin-orbit state of the Br atoms probed. Previous experiments[12–14] have confirmed that the difference between photodissociation cross sections at closely spaced REMPI lines can be neglected.

A. 234 nm photodissociation of 1-bromo-2-butene

1. Translational energy distribution

Ion images of the $Br(^2P_{3/2})$ and $Br(^2P_{1/2})$ photofragments are shown in Fig. 2(a) and 2(b), respectively, with the 234 nm laser polarization direction in the vertical axis. Each image displays a single high-kinetic-energy release component. The speed distributions of the $Br(^2P_{1/2,3/2})$ fragments are extracted by integrating the three-dimensional speed distributions over all solid angles at each speed and the total center-of-mass translational energy distributions, $P(E_T)$'s, are derived from the $Br(^2P_{1/2,3/2})$ atom speed distributions using conservation of momentum and correcting for the appropriate Jacobian. The results are presented in Fig. 3, where the peak value of translational energy release in the C–Br fission channel which produces $Br(^2P_{3/2})$ atoms is 30.5 kcal/mol and that producing $Br(^2P_{1/2})$ is 26.0 kcal/mol. The C–Br bond fission proceeds on a repulsive electronic state, and the lower recoil kinetic energies in the $Br(^2P_{1/2})$ channel likely reflect the lower available energy for that channel due to the substantial (10.54 kcal/mol) spin-orbit splitting between the $^2P_{3/2}$ and $^2P_{1/2}$ states of the Br atoms. The difference (4.5 kcal/mol) is smaller than the actual $Br(^2P_{1/2})/Br(^2P_{3/2})$ spin-orbit energy. Nevertheless, less internal energy is partitioned into the 1-methylallyl radical cofragments in the channel producing $CH_2CH{=}CHCH_3+Br(^2P_{1/2})$. This is also true for the C_4H_7 radical cofragments formed in the higher spin-orbit state channel in the photodissociation of cyclobutyl bromide, cyclopropylmethyl bromide (see Sec. III B 1), and 4-bromo-1-butene (see Sec. III D 1).

The raw image of 1-methylallyl radicals taken at 234 +157 nm are shown in Fig. 4. Both 157 nm and 234 nm lasers can photodissociate the 1-methylallyl bromide molecules, but only the 157 nm photons are energetic enough to ionize the 1-methylallyl radicals. We found that there is no observable signal from the 157 nm laser alone so no back-

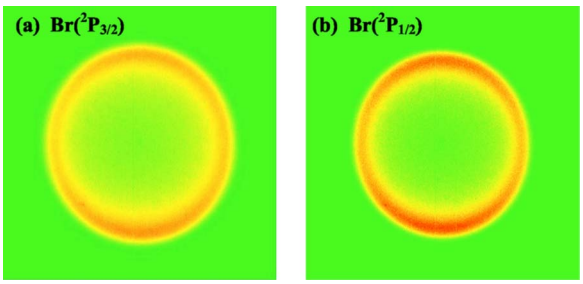

FIG. 2. (Color online) Raw images (a) $Br(^2P_{3/2})$ obtained at 233.681 nm and (b) $Br(^2P_{1/2})$ obtained at 234.021 nm from the C–Br bond fission of 1-bromo-2-butene. The laser polarization is along the vertical direction in the plane of the images. Each image consists of 861×861 pixels and is constructed by accumulating signals from ~200 000 laser shots. The distance of 1.0 cm on the phosphor screen corresponds to the width of 221.6 pixels in the images and 882 m/s Br atom recoil velocity.

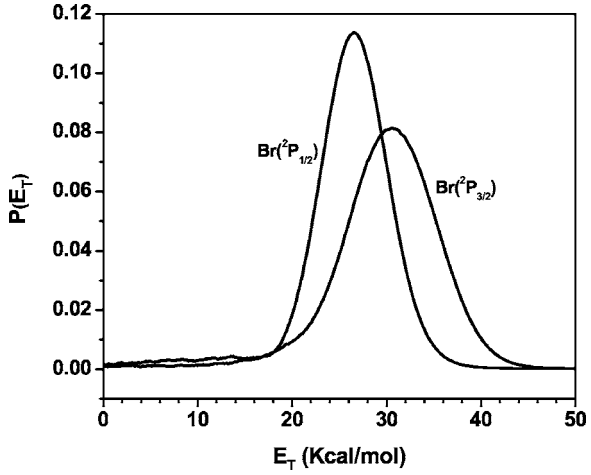

FIG. 3. The $P(E_T)$'s of 1-methylallyl+$Br(^2P_{1/2})$ and 1-methylallyl +$Br(^2P_{3/2})$ derived from Fig. 2.

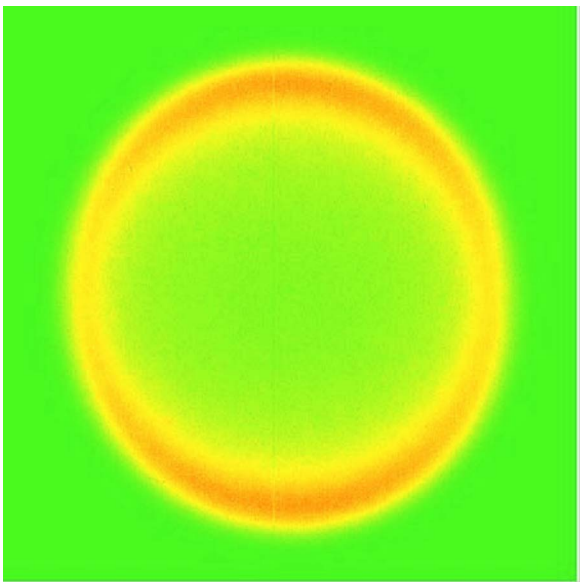

FIG. 4. (Color online) Raw image of the 1-methylallyl radical from the C–Br bond fission of 1-bromo-2-butene at 234+157 nm. There is no noticeable signal at 157 nm only. Each image has a dimension of 861 ×861 pixels.

ground signal subtraction is required. The resultant $P(E_T)$ is displayed as the solid curve in Fig. 5. The total recoil translational energy release in these processes spans the range of 15–42 kcal/mol and peaks at around 26.0 kcal/mol. Based on conservation of energy, the 1-methylallyl radicals produced in the 234 nm photodissociation of 1-bromo-2-butene have an internal energy distribution that ranges from 7 to near 30 kcal/mol [the highest internal energy radicals are formed primarily in conjunction with $Br(^2P_{3/2})$]. As shown in Fig. 1, the 1-methylallyl radical can only isomerize to 3-buten-2-yl ($CH_2{=}CHCH_2CH_2$) and/or dissociate to 1,3-butadiene+H by surmounting barriers over 48 kcal/mol relative to 1-methylallyl. Thus, the 1-methylallyl radicals generated by the C–Br bond cleavage of 1-methylallyl bromide, having an internal energy ranged from 7 to near

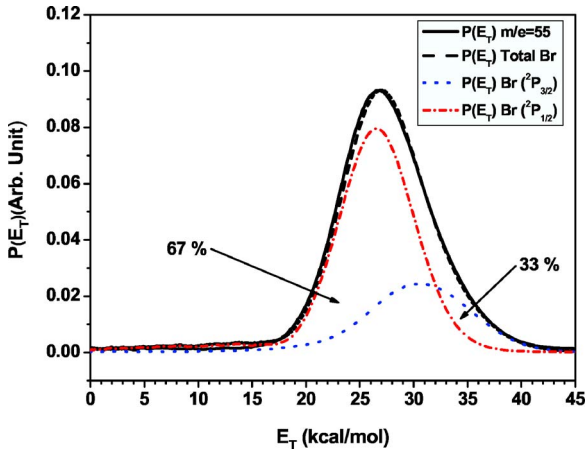

FIG. 5. (Color online) The C–Br fission $P(E_T)$ derived from the 1-methylallyl radical data in Fig. 4 is shown in solid line. The dashed line shows the best fit C–Br fission $P(E_T)$ obtained from the weighted sum of the individual Br distributions in Fig. 3 (those weighted contributions are shown in dotted and dot-dashed line).

30 kcal/mol, are very likely to be stable in the potential energy well. This allows us to determine the spin-orbit branching ratio and REMPI line strength without any ambiguity.

2. Spin-orbit branching ratio and REMPI line strength

This study focuses on the C–Br bond fission to yield C_4H_7 and $Br(^2P_{1/2,3/2})$ photofragments; other sources of producing atomic Br fragments such as the secondary photodissociation of HBr (produced from the primary photodissociation channel of $C_4H_7Br \rightarrow C_4H_6+HBr$) are assumed to be negligible. The spin-orbit branching ratio is determined by matching the total C–Br bond fission $P(E_T)$ from the kinetic energy measurement of Br atoms, constructed by a weighted sum of the $P(E_T)$'s derived from the individual $Br(^2P_{3/2})$ and $Br(^2P_{1/2})$ fragments, to the $P(E_T)$ determined from the C_4H_7 fragments. The normalized $P(E_T)$'s of both $Br(^2P_{3/2})$ and $Br(^2P_{1/2})$ atoms were first added together with an arbitrary weighting factor. The total C–Br bond fission $P(E_T)$ derived was then compared with the $P(E_T)$ of C_4H_7 fragments. The weighting factor is then adjusted accordingly until a good agreement between the total $P(E_T)$ from the Br fragments and the $P(E_T)$ determined from the C_4H_7 is reached. The best fit contribution of the $Br(^2P_{1/2})$ and $Br(^2P_{3/2})$ $P(E_T)$'s to the total $P(E_T)$'s for C–Br bond fission in 1-methylallyl bromide is displayed in Fig. 5 with the dashed line for the $P(E_T)$ determined from the Br atoms and the solid line for the $P(E_T)$ determined from the 1-methylallyl signal. This corresponds to a branching ratio for $Br(^2P_{1/2}):Br(^2P_{3/2})$ $=2.03\pm0.05$. The uncertainty of 0.05 represents the standard deviation calculated from fitting the $P(E_T)$'s from several different imaging measurements.

In a typical ion imaging experiment involving halogen photofragments, the REMPI line strength factor is crucial in determining the spin-orbit branching ratio. As mentioned previously, the REMPI line strength factor determined by momentum match between the Br atoms and the c-C_4H_7 radical cofragments in the C–Br bond fission of cyclobutyl bromide may be unreliable because there are multiple possible photoionization channels for the c-C_4H_7 radical and the branching to the $Br(^2P_{1/2})$ channel is small. The current experiment allows us to more accurately determine this relative line strength for 2+1 REMPI detection of Br atoms at the wavelengths of 233.681 and 234.021 nm. The spin-orbit branching ratio $N[Br(^2P_{1/2})]/N[Br(^2P_{3/2})]$ is proportional to the measured ion signal ratio $S[Br(^2P_{1/2})]/S[Br(^2P_{3/2})]$ according to the following equation:

$$N[Br(^2P_{1/2})]/N[Br(^2P_{3/2})] = k \times S[Br(^2P_{1/2})]/S[Br(^2P_{3/2})], \quad (4)$$

where $N(X)$ is the number of bromine atoms produced in the photodissociation event, $S(X)$ is the measured bromine ion signal intensity, and k is the relative REMPI line strength ratio at the $Br(^2P_{3/2})$ and $Br(^2P_{1/2})$ detection wavelengths. The spin-orbit branching ratio of $Br(^2P_{1/2})$ to $Br(^2P_{3/2})$ from the photodissociation of 1-methylallyl bromide at 234 nm has already been determined as described above to be 2.03 ± 0.05; the only parameter needed is the bromine ion

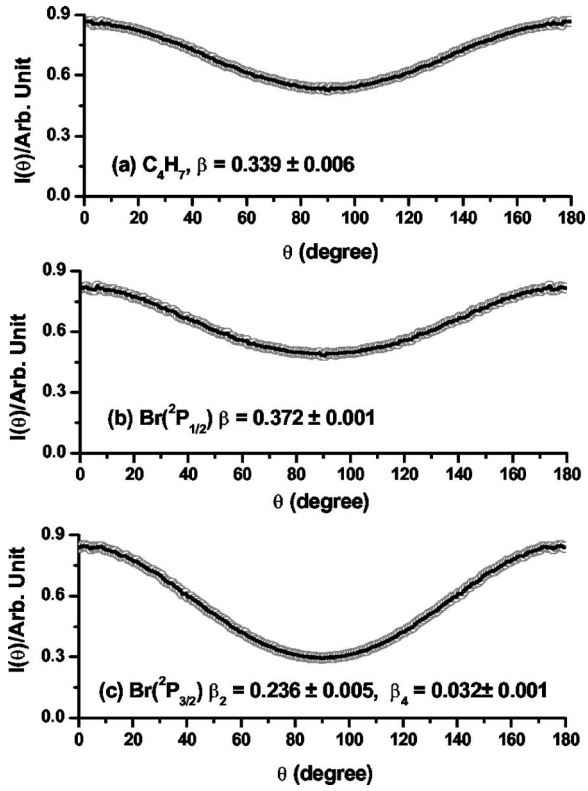

FIG. 6. Angular distribution fitting of (a) 1-methylallyl radical, (b) $Br(^2P_{1/2})$, and (c) $Br(^2P_{3/2})$ formed in the C–Br bond fission of 1-bromo-2-butene.

signal intensity ratio. The total $m/e=79$ ion signal intensity is obtained by integrating the time-of-flight profile at the appropriate time window displayed on the oscilloscope where the signals are directly collected from the phosphor screen. The ratio $S[Br(^2P_{1/2})]/S[Br(^2P_{3/2})]$ is measured to be 12.27. (Here the laser is set to a wavelength which maximizes the signal, so does not probe the entire Doppler profile.) Plugging this and a $N[Br(^2P_{1/2})]/N[Br(^2P_{1/2})]$ value of 2.03 into the above equation, the constant k, i.e., the relative REMPI line strength of $Br(^2P_{3/2})$ to $Br(^2P_{1/2})$, is calculated to be 0.17 ± 0.05. The present REMPI line strength for $Br(^2P_{3/2})$ to $Br(^2P_{1/2})$ obtained from weighting the $P(E_T)$'s calculated from the Br atomic fragments until it compared closely to the $P(E_T)$ derived from velocity measurements of the 1-methylallyl radical cofragments is slightly larger but still within the error range of the REMPI line strength of 0.10 ± 0.07 (obtained from the same procedure with the Br and cyclobutyl fragments) in the previous photodissociation study on cyclobutyl bromide.[14] The difference between these two measurements is discussed in Sec. III C.

3. Photofragment angular distributions

The use of a linearly polarized laser to photolyze 1-bromo-2-butene and probe the $Br(^2P_{1/2})$ and $Br(^2P_{3/2})$ atomic fragments with the same laser beam yields the product recoil angular distributions shown in Figs. 6(b) and 6(c), respectively. The $Br(^2P_{1/2})$ angular distribution, Fig. 6(b), is fit using the following expression:

$$I(\theta) \propto 1 + \beta P_2(\cos\theta), \tag{5}$$

where θ is the angle between the product recoil velocity and the polarization axis of the photolysis laser. $I(\theta)$ is the integrated signal over a certain speed range at angle θ and $P_2(\cos\theta)$ is the second-order Legendre polynomial. An anisotropy parameter of 0.372 ± 0.001 (the uncertainty is assigned based on the standard error from repeated measurements) is obtained for $Br(^2P_{1/2})$ with the signal integrated over the translational energy range of 13–40 kcal/mol, indicating a slightly parallel distribution. (The anisotropy parameter β can range from −1 to +2, with −1 corresponding to perpendicular transition and +2 corresponding to parallel transition upon photoexcitation of the parent molecules.)

The angular distribution for the ground state bromine [Fig. 6(c)], however, cannot be fit by Eq. (5). The $Br(^2P_{3/2})$ atoms, having spin-orbit angular momentum quantum number (J) larger than 1/2, may have an aligned m_J distribution that can influence the efficiency of the linearly polarized REMPI process.[18–20] The detected $Br(^2P_{3/2})$ angular distribution in Fig. 6(c) is thus fitted by

$$I(\theta) \propto 1 + \beta_2 P_2(\cos\theta) + \beta_4 P_4(\cos\theta). \tag{6}$$

Note that the coefficient β_2 in the above equation is influenced by the laboratory frame quadrupole alignment A_0 as well as the photofragment angular distribution, therefore is not equal to the spatial anisotropy parameter β in Eq. (5). By integrating the signal for $Br(^2P_{3/2})$ over the translational energy range of 13–45 kcal/mol, we obtained anisotropy parameters $\beta_2=0.236\pm0.005$ and $\beta_4=0.032\pm0.001$.

Similar to our analysis for the $Br(^2P_{1/2})$ fragments, an anisotropy parameter $\beta=0.339\pm0.006$ for the 1-methylallyl radical is obtained by integrating the signal over the translational energy range of 15–45 kcal/mol and fitting with Eq. (5). On the basis of momentum conservation, the angular distribution of the 1-methylallyl radical would precisely match with that of the $Br(^2P_{1/2})$ and $Br(^2P_{3/2})$ cofragments. The anisotropy parameter characterizing the total angular distribution for both $Br(^2P_{1/2})$ and $Br(^2P_{3/2})$ fragments could be obtained by the weighted sum of the anisotropy parameters $\beta=0.372\pm0.001$ for $Br(^2P_{1/2})$ and the β for the $Br(^2P_{3/2})$ channel with the spin-orbit branching ratio $[Br(^2P_{1/2}):Br(^2P_{3/2})=2.03\pm0.05]$ determined in Sec. III A 2 and should be the same as that derived from the 1-methylallyl radicals. However, calculating the anisotropy parameter for the $Br(^2P_{3/2})$ channel from the measured β_2 and β_4 parameters is precluded by the possibility that the photofragment alignment is not independent of the Br atom recoil direction.

B. 234 nm photodissociation of cyclopropylmethyl bromide

1. Translational energy distribution

The respective ion images of the $Br(^2P_{3/2})$ and $Br(^2P_{1/2})$ photofragments in the C–Br bond fission of cyclopropylmethyl bromide are shown in Figs. 7(a) and 7(b). Each image similarly displays a single high-kinetic-energy release component. The speed distributions of the $Br(^2P_{1/2,3/2})$ fragments are extracted by integrating the three-dimensional speed dis-

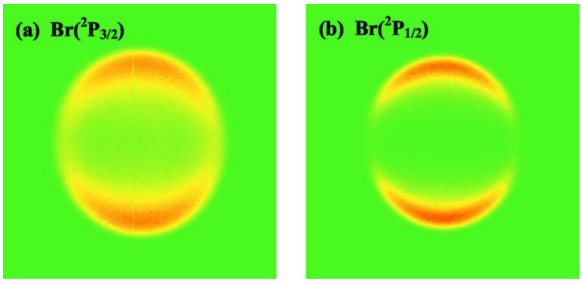

FIG. 7. (Color online) Raw images (a) Br($^2P_{3/2}$) obtained at 233.681 nm and (b) Br($^2P_{1/2}$) obtained at 234.021 nm from the C–Br bond fission of cyclopropylmethyl bromide. The laser polarization is along the vertical direction in the plane of the images. Each image consists of 861 $\times$ 861 pixels and is constructed by accumulating signals from ~200 000 laser shots. The distance of 1.0 cm on the phosphor screen corresponds to the width of 221.6 pixels in the images and 882 m/s Br atom recoil velocity.

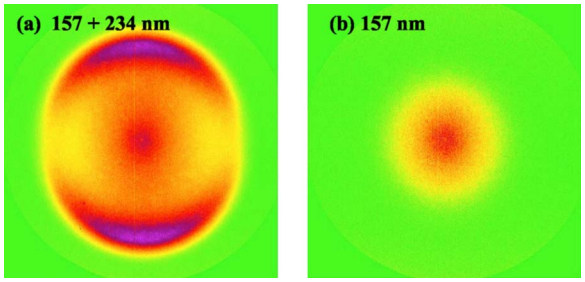

FIG. 9. (Color online) Raw images of the cyclopropylmethyl radical from the C–Br bond fission of cyclopropylmethyl bromide (a) at 234+157 nm and (b) at 157 nm. A high-translational energy component appearing in (a) but not in (b) reveals that the contribution of cyclopropylmethyl fragments from 234 photodissociation with the radicals ionized by the 157 nm photons. Each image has a dimension of 861 $\times$ 861 pixels.

tributions over all solid angles at each speed and the total center-of-mass translational energy distributions, $P(E_T)$'s, are derived from the Br($^2P_{1/2,3/2}$) atom speed distributions using conservation of momentum and correcting for the appropriate Jacobian. The results are presented in Fig. 8, where the peak value of translational energy release in the C–Br fission channel which produces Br($^2P_{3/2}$) atoms is 25.5 kcal/mol and that producing Br($^2P_{1/2}$) is 22.0 kcal/mol. Similar to the 1-bromo-2-butene and cyclobutyl bromide, relatively less internal energy is partitioned into the channel producing excited spin-orbit state Br($^2P_{1/2}$) and cyclopropylmethyl radical photofragments.

The raw images of cyclopropylmethyl photofragments taken at 234+157 and 157 nm are shown in Figs. 9(a) and 9(b), respectively. A high-recoil-kinetic-energy cyclopropylmethyl component is found in the polar region of the image at 234+157 nm, corresponding to the cyclopropylmethyl fragments formed in the 234 nm photodissociation and probed by the 157 nm photons. At the center region of images in Fig. 9(a) and 9(b), a weak and low-kinetic-energy component due to the cyclopropylmethyl cations formed in 157 nm photodissociation/photoionization is observed, but these signals are very well separated from the cyclopropylmethyl radicals formed from 234 nm photodissociation. Both the 157 and the 234 nm lasers can photodissociate the cyclopropylmethyl bromide molecules, but only the 157 nm photons are energetic enough to ionize the cyclopropylmethyl radicals (the IE is about 7.0 eV). Thus the $P(E_T)$ of the $m/e=55$ signal from 234 nm photodissociation can be obtained by subtracting the signal at 157 nm from the signal at 234+157 nm. The resultant $P(E_T)$ after subtraction is displayed as the solid curve in Fig. 10. The total recoil translational energy release in these processes spans the range of 10–40 kcal/mol and peaks at approximately 25.0 kcal/mol. Based on conservation of energy, the cyclopropylmethyl radicals produced in the 234 nm C–Br bond fission of cyclopropylmethyl bromide have an internal energy distribution that ranges from 15.8 to 45.8 kcal/mol.

The electronic structure predictions in Fig. 1 show that the cyclopropylmethyl radical could undergo isomerization to form cyclobutyl radical via a transition barrier of 47.6 kcal/mol or a ring-opening isomerization to form 3-buten-1-yl radical and further dissociate into hydrogen and C_4H_6 via a barrier of 24.8 kcal/mol (relative to the zero-point level of the cyclopropylmethyl radical). The dissociation to form H+1,3-C_4H_6 is the lowest unimolecular dissociation pathway governing the reactivity of cyclopropylmethyl radical on the C_4H_7 potential energy surface.

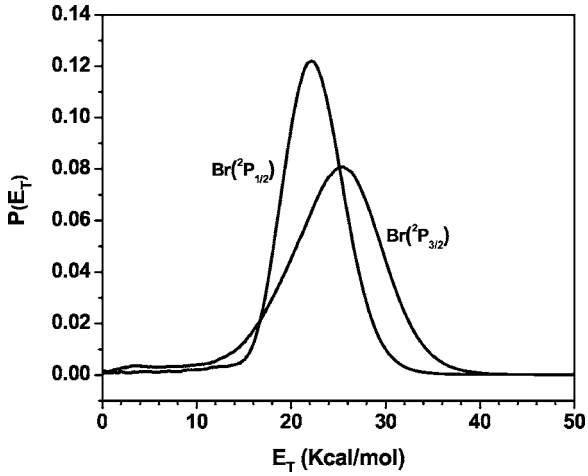

FIG. 8. The $P(E_T)$'s of cyclopropylmethyl+Br($^2P_{1/2}$) and cyclopropylmethyl+Br($^2P_{3/2}$) derived from Fig. 7.

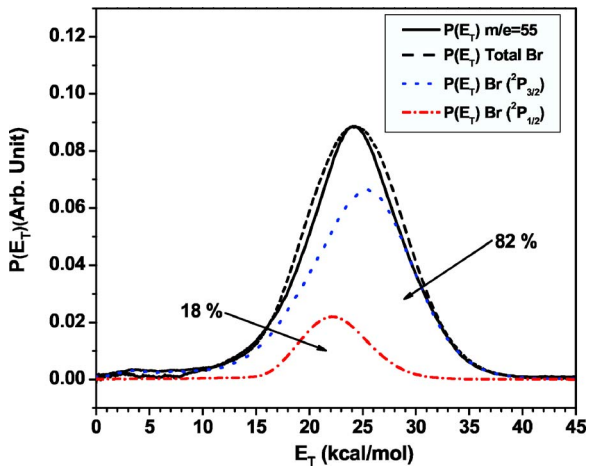

FIG. 10. (Color online) The $P(E_T)$ of cyclopropylmethyl radical derived from Fig. 9 (shown in solid line). The dashed line $P(E_T)$ is obtained from the weighted sum of the individual Br distributions in Fig. 8 using the line strength ratio determined in this work.

Thus, one would expect that cyclopropylmethyl radicals formed with internal energy more than ~25 kcal/mol should be unstable to isomerization in the formation of 3-buten-1-yl radical and followed by the elimination to form H and 1,3-C_4H_6. In contrast, our experiment detects the $m/e=55$ ion signal with internal energies as high as 45.8 kcal/mol. This stability at internal energies higher than the dissociation barrier can result if a significant fraction of the C–Br fission events releasing between 15.8 and 45.8 kcal/mol to internal energy of the cyclopropylmethyl radicals have partitioned enough of this remaining energy to rotation rather than vibration to leave the radical with a vibrational energy less than the ~25 kcal/mol barrier to isomerization. For example, assuming the recoil velocity vector is along the C–Br bond direction at the equilibrium ground state geometry of cyclopropylmethyl bromide, an impulsive dissociation imparting 31 kcal/mol into relative kinetic energy would impart 18.3 kcal/mol of energy into relative rotational energy of cyclopropylmethyl radical, by the conservation of angular momentum, leaving the cyclopropylmethyl radicals (for the ones formed in conjunction with ground spin-orbit state Br atoms and having a total internal energy of 24.8 kcal/mol) with too little vibrational energy to isomerize and dissociate. This angular momentum conservation thus explains why most of the radicals formed with more than 25 kcal/mol internal energy do not dissociate to H+1,3-C_4H_6, but it leaves the survival of radicals produced with the lowest recoil kinetic energies unexplained.

2. Spin-orbit branching ratio

Measured from the TOF signals of Br fragments, the $Br(^2P_{1/2})$ to $Br(^2P_{3/2})$ ion signal intensity ratio (i.e., $S[Br(^2P_{1/2})]/S[Br(^2P_{3/2})]$) is determined to be 1.295:1. Multiplying this intensity ratio by the line strength factor (k) determined in Sec. III A 2 gives a branching ratio of 0.22:1 for the C–Br fission events of the cyclopropylmethyl bromide producing $Br(^2P_{1/2})$ to the C–Br fission events producing $Br(^2P_{3/2})$. In other words, 82% of the C–Br bond fission events produce $Br(^2P_{3/2})$ and 18% of the C–Br fission events produce $Br(^2P_{1/2})$. To obtain a total $P(E_T)$ distribution for production of the cyclopropylmethyl radicals, we first normalize the $P(E_T)$'s for the production of each Br spin-orbit state shown in Fig. 8, then calculate the weighted sum of these $P(E_T)$'s which is equal to $0.82\times P(E_T)$ for producing $Br(^2P_{3/2})$ plus $0.18\times P(E_T)$ for producing $Br(^2P_{1/2})$. The $P(E_T)$ distribution thus obtained for the C–Br fission events producing all the Br atomic fragments is plotted in Fig. 10 with dashed line. As it clearly shown in Fig. 10, the $P(E_T)$ for the C–Br fission events producing the Br atomic fragments is almost perfectly matched with the $P(E_T)$ (in solid curve) for the C–Br fission events derived from the velocity distribution of the cyclopropylmethyl radical cofragments detected using 157 nm photoionization and detected as $m/e=55$ ions. Only the widths of the $P(E_T)$ distributions are slightly mismatched. Note that the only adjustable parameter in the above fitting procedure is the line strength factor (k) determined in Sec. III A 2, so the very close correspondence between the solid line $P(E_T)$ derived from the photoionized cyclopropylmethyl fragments and the dashed line $P(E_T)$ from weighting the two Br atom distributions shows both that the line strength factor is adequate and that the photoionization cross section of the cyclopropylmethyl radical is relatively insensitive to internal energy. As the cyclopropylmethyl cation is structurally similar to the cyclopropylmethyl radical (indicated by the vertical IE comes fairly close to the adiabatic IE value), we expect that the Franck-Condon factor for the photoionization of the cyclopropylmethyl radical near its ionization threshold is very favorable. Thus, the $m/e=55$ ion signals we observed should directly come from the 157 nm photoionization of cyclopropylmethyl radicals, generated in the C–Br fission of cyclopropylmethyl bromide, yielding the cyclopropylmethyl cation. One might have thought that since many of these radicals are subject to isomerization to 3-buten-1-yl radicals that we might also observe photoionization from that isomer, but our work on that system later in this paper suggests that the photoionization cross section from that isomer is very small.

3. Photofragment angular distribution

Similar to our angular distribution analysis on 1-bromo-2-butene, we used Eqs. (5) and (6) to fit the angular distribution of the $Br(^2P_{1/2})$ and $Br(^2P_{3/2})$ fragments, respectively. Integrating the signal over the translational energy range of 11–32 kcal/mol for the $P(E_T)$ of $Br(^2P_{1/2})$ fragments gives an anisotropy parameter of $\beta=1.640\pm0.021$ (the uncertainty is assigned based on the standard error from repeated measurements). By integrating the signals for the $P(E_T)$ of $Br(^2P_{3/2})$ fragments over the translational energy range of 10–40 kcal/mol, we have determined that the anisotropy parameters for the angular distribution of the $Br(^2P_{3/2})$ are $\beta_2=0.775\pm0.016$ and $\beta_4=0.032\pm0.003$. Both fittings for the angular distribution of $Br(^2P_{1/2})$ and $Br(^2P_{3/2})$ fragments are displayed in Fig. 11. To obtain the anisotropy fitting parameter characterizing the angular distribution of cyclopropylmethyl radicals, we have integrated the signal over the translational energy range of 10–40 kcal/mol and obtained a β value of 0.902 ± 0.034. The angular distribution of the cyclopropylmethyl radicals must precisely match that of the weighted sum of the $Br(^2P_{1/2})$ and $Br(^2P_{3/2})$ cofragments (as these fragments are produced in the same C–Br bond fission events). The anisotropy parameter of the total angular distribution for both $Br(^2P_{1/2})$ and $Br(^2P_{3/2})$ fragments could be obtained by the weighted sum of the anisotropy parameters $\beta=1.640\pm0.021$ for $Br(^2P_{1/2})$ and the corresponding β for the $Br(^2P_{3/2})$. We attempted to derive an approximate value for the β for the $Br(^2P_{3/2})$ channel from the measured values of $\beta_2=0.775\pm0.016$ and $\beta_4=0.032\pm0.003$ by solving the expressions in Eq. (11) of Ref. 20. This gave an approximate β of 0.673 ± 0.016 for the $Br(^2P_{3/2})$ channel, but note that the use of the expression in that reference depended on the relative photofragment alignment with respect to recoil direction as explained in Ref. 21. Weighting the measured β for the $Br(^2P_{1/2})$ channel and the approximate β for the $Br(^2P_{3/2})$ channel by the spin-orbit branching ratio $[Br(^2P_{1/2}):Br(^2P_{3/2})=0.18:0.82]$ determined in Sec. III B 2 gives an anisotropy parameter of β

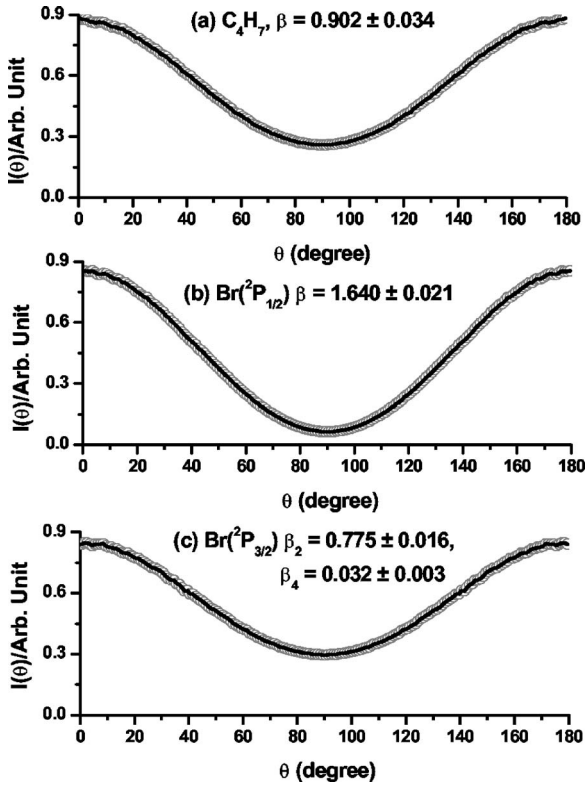

FIG. 11. Angular distribution fitting of (a) cyclopropylmethyl radical, (b) Br($^2P_{1/2}$), and (c) Br($^2P_{3/2}$) formed in the C–Br bond fission of cyclopropylmethyl bromide.

$=0.846\pm0.023$ for the total C–Br fission angular distribution. This compares closely with the β of 0.902 ± 0.034 for the momentum-matched cyclopropylmethyl fragments, with the difference likely due to a recoil dependent alignment of the Br($^2P_{3/2}$) fragments.

C. Revisiting cyclobutyl bromide and the REMPI line strength deduction

In the present study, we have deduced a new REMPI line strength of 0.17 ± 0.05 for Br($^2P_{3/2}$) to Br($^2P_{1/2}$) from the velocities of the momentum-matched Br atomic fragments and 1-methylallyl radical cofragments. This value is slightly larger than the previous REMPI line strength of 0.10 ± 0.07 obtained from doing a similar analysis on the Br atoms and cyclobutyl cofragments in our prior imaging studies of cyclobutyl bromide photodissociation. That data had only a small contribution from the Br($^2P_{1/2}$) channel, so the overall fit to obtain the total $P(E_T)$ was not strongly sensitive to the fraction of Br($^2P_{1/2}$) included. Using the newly deduced REMPI line strength of 0.17 ± 0.05, Fig. 12 shows the $P(E_T)$ for the C–Br bond fission of cyclobutyl bromide producing the total Br atomic fragments and the original $P(E_T)$ for the C–Br bond fission producing cyclobutyl cofragments. The original $P(E_T)$'s for the C–Br bond fission of cyclobutyl bromide producing cyclobutyl radicals and the total Br atomic fragments used to deduce the previous REMPI line strength of 0.10 ± 0.07 have been reported previously.[14] Comparing Fig. 12 in this article and Fig. 4 in Ref. 14 reveals that the C–Br fission producing total Br atomic fragments with the newly deduced REMPI line strength features a slightly

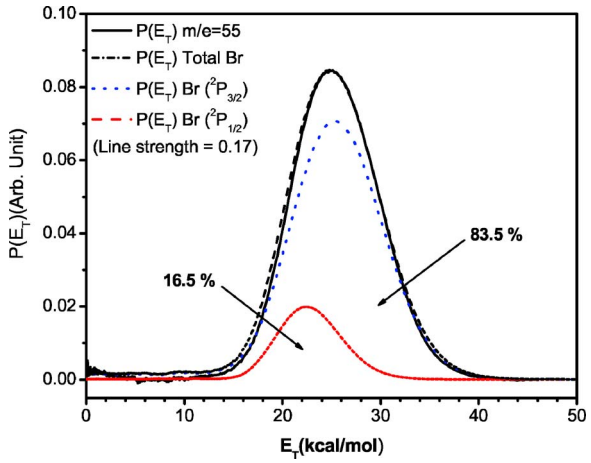

FIG. 12. (Color online) The $P(E_T)$ of cyclobutyl radical is taken from Ref. 14 (shown in solid line). The $P(E_T)$ (dotted line) is obtained from the weighted sum of the individual Br distributions using the newly deduced REMPI line strength factor.

slower $P(E_T)$ than that with the previous REMPI line strength; the peak of the $P(E_T)$ is shifted to lower kinetic energy by 0.2 kcal/mol and the slow side of the $P(E_T)$ is mismatched slightly, but these differences are within our measurement error. The determination of the REMPI line strength by measuring the $P(E_T)$ for the cyclobutyl radicals and momentum match with the $P(E_T)$ for the total Br cofragments could be unreliable because the photoionization of cyclobutyl radical at a photon energy of 7.9 eV may have multiple ionization products. The cyclobutyl radical could ionize into three possible cyclobutyl cations with significantly different structures in the IEs ranged from 7.0 to 7.6 eV, one would expect that Franck-Condon overlap for the photoionization process in yielding a cationic structure similar to its initial neutral structure should be more favorable than that in yielding a cationic structure significantly different from the initial neutral structure. Thus, we favor the line strength ratio derived in this current work from the Br atoms and momentum-matched 1-methylallyl radicals. Note also one typographical error in the cyclobutyl bromide paper; the approximate anisotropy parameter derived for the Br($^2P_{3/2}$) fragments from the measured β_2 and β_4 should have been given as 1.19, not 1.12.

D. 234 nm photodissociation of 4-bromo-1-butene

1. Translational energy distribution

Raw images of the Br($^2P_{3/2}$) and Br($^2P_{1/2}$) photofragments for the C–Br bond fission of 4-bromo-1-butene are shown in Figs. 13(a) and 13(b), respectively, with the laser polarization direction in the vertical axis. Both the Br($^2P_{3/2}$) and Br($^2P_{1/2}$) images indicate that there is an intense high-recoil-kinetic-energy component in the polar region. After appropriate transformation, the resulting $P(E_T)$ distributions are displayed in Fig. 14. The C–Br fission channel producing Br($^2P_{3/2}$) peaks at a translational energy release of 25.0 kcal/mol while that producing Br($^2P_{1/2}$) peaks at 22.0 kcal/mol. Similar to 1-bromo-2-butene, C–Br bond fission proceeds on a repulsive electronic state such that the lower recoil kinetic energies in the Br($^2P_{1/2}$) channel likely

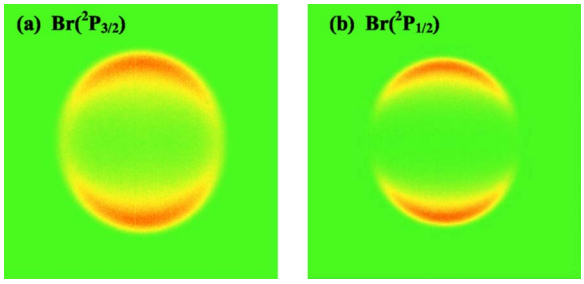

FIG. 13. (Color online) Raw images (a) Br($^2P_{3/2}$) obtained at 233.681 nm and (b) Br($^2P_{1/2}$) obtained at 234.021 nm from the C–Br bond fission of 4-bromo-1-butene. The laser polarization is along the vertical direction in the plane of the images. Each image consists of 861×861 pixels and is constructed by accumulating signals from ~200 000 laser shots. The distance of 1.0 cm on the phosphor screen corresponds to the width of 221.6 pixels in the images and 882 m/s Br atom recoil velocity.

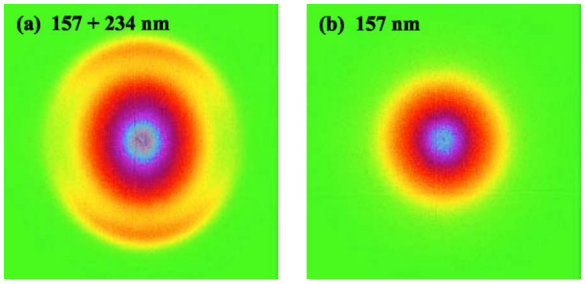

FIG. 15. (Color online) Raw image of the $m/e=55$ radical from the C–Br bond fission of 4-bromo-1-butene (a) at 234+157 nm and (b) at 157 nm. A high-translational energy component appearing in (a) but not in (b) reveals that the contribution of $m/e=55$ fragments from 234 photodissociation and followed by the 157 nm photoionization. Each image has a dimension of 861×861 pixels.

reflect the lower available energy for that channel due to the substantial (10.54 kcal/mol) spin-orbit splitting between the $^2P_{3/2}$ and $^2P_{1/2}$ states of the Br atoms. The difference (3.0 kcal/mol) is notably smaller than the actual Br($^2P_{1/2}$)/Br($^2P_{3/2}$) spin-orbit splitting, and less internal energy is partitioned into the 3-buten-1-yl radical cofragments in the channel producing $CH_2CHCH_2CH_2$+Br($^2P_{1/2}$).

The raw images of the 3-buten-1-yl photofragments taken at 234+157 nm and 157 nm are shown in Figs. 15(a) and 15(b), respectively. A high-recoil-kinetic-energy 3-buten-1-yl component is found in the polar region of the image at 234+157 nm, corresponding to the 3-buten-1-yl radical fragments formed in the 234 nm photodissociation and probed by the 157 nm photons. At the center region of both images, an intense and low-kinetic-energy component due to the C_4H_7 cations formed in the 157 nm photodissociation/photoionization is observed; these signals have a small overlap with the faster recoiling 3-buten-1-yl radicals formed in the 234 nm photodissociation. Both 157 and 234 nm lasers can photodissociate the 4-bromo-1-butene molecules, but only the 157 nm photons are energetic enough to ionize the 3-buten-1-yl radicals (see Table II for IE value). Thus the $P(E_T)$ of the $m/e=55$ signal from 234 nm photodissociation can be obtained by subtracting the signal at 157 nm from the signal at 234+157 nm. The resultant $P(E_T)$ after subtraction is displayed as the solid curve in Fig. 16. The total recoil translational energy release in the C–Br fission processes that produce radicals that we can detect using 157 nm photoionization spans in the range of 14–32 kcal/mol and peaks at approximately 22 kcal/mol. Based on conservation of energy, the 3-buten-1-yl radicals produced in the 234 nm C–Br bond fission of 4-bromo-1-butene which are able to be detected with photoionization at 157 nm are a subset of all the radicals produced, and those radicals have an internal energy ranging from 22.5 to 40.5 kcal/mol. In contrast, the $P(E_T)$ derived from the weighted sum of the momentum-matched Br($^2P_{3/2}$) and Br($^2P_{1/2}$) cofragments shows significant signal at higher recoil kinetic energies, giving an internal energy distribution of 3-buten-1-yl radicals produced in the 234 nm C–Br bond fission of 4-bromo-1-butene as ranging from 19 to 40 kcal/mol (see Fig. 16). Clearly the 3-buten-1-yl radicals formed in higher recoil kinetic energy C–Br fission events, the 3-buten-1-yl radicals with the lowest internal energies, are not being efficiently photoionized with 157 nm photons. We return to this observation in the next section.

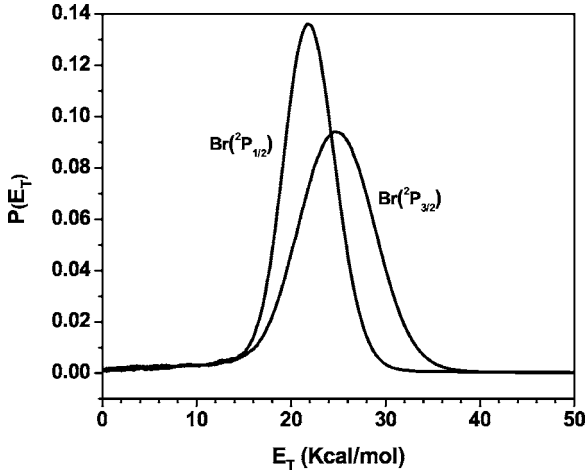

FIG. 14. The $P(E_T)$'s of 3-buten-1-yl+Br($^2P_{1/2}$) and 3-buten-1-yl +Br($^2P_{3/2}$) derived from Fig. 13.

2. Spin-orbit branching ratio and internal energy distribution of the 3-buten-1-yl radical

Measured from the TOF signals of Br fragments, the Br($^2P_{1/2}$) to Br($^2P_{3/2}$) ion signal intensity ratio (i.e., S[Br($^2P_{1/2}$)]/S[Br($^2P_{3/2}$)]) is determined to be 1.174:1. Mul-

TABLE II. The adiabatic and vertical IEs (in eV) calculated at the G3//B3LYP level for each individual C_4H_7 radical generated in this study.

	Adiabatic IE	Vertical IE[a]
trans-$CH_2CH{=}CHCH_3 \rightarrow$ *trans*-$CH_2CH{=}CHCH_3^+$	7.51	7.57
cis-$CH_2CH{=}CHCH_3 \rightarrow$ *cis*-$CH_2CH{=}CHCH_3^+$	7.62	7.66
c-$CH_2{-}CHCH_2CH_2 \rightarrow$ *c*-$CH_2{-}CHCH_2CH_2^+$	7.04	7.54
trans-$CH_2{=}CHCH_2CH_2 \rightarrow$ *trans*-$CH_2CH{=}CHCH_3^+$	6.82	8.56[b]
cis-$CH_2{=}CHCH_2CH_2 \rightarrow$ *cis*-$CH_2CH{=}CHCH_3^+$	6.93	8.56[b]

[a]Vertical IE is calculated as the G3//B3LYP energy difference (without zero-point vibrational energy) between the radical and cation. The optimized structures of the neutral radicals at the B3LYP/6-31G(d) level are used.
[b]These vertical ionization transitions correspond to *cis*-/*trans*-3-buten-1-yl radical ionizing to *cis*-/*trans*-3-buten-1-yl cation.

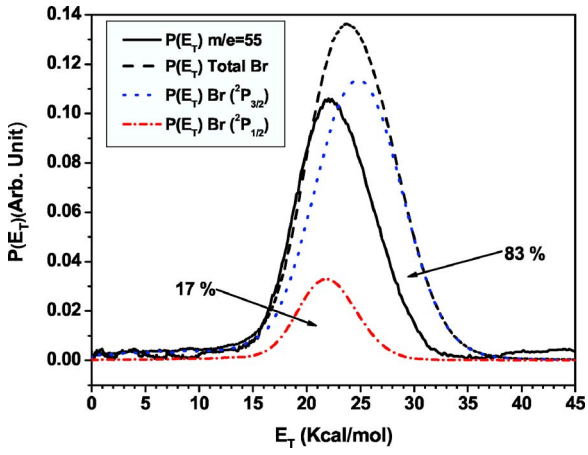

FIG. 16. (Color online) The partial C–Br fission $P(E_T)$ shown in solid line is derived from the velocities of the $m/e=55$ radicals detected using 157 nm photoionization, shown in Fig. 15. The C–Br fission $P(E_T)$ shown in dashed line is obtained from the weighted sum of the individual Br distributions in Fig. 14 (shown in dotted line and dot-dashed line).

tiplying this intensity ratio by the line strength factor (k) determined in Sec. III A 2 gives a branching ratio of 0.20:1 for the C–Br fission events of the 4-bromo-1-butene producing $Br(^2P_{1/2})$ to the C–Br fission events producing $Br(^2P_{3/2})$. Thus, 83% of the C–Br bond fissions produce $Br(^2P_{3/2})$ and 17% of the C–Br bond fission events produce $Br(^2P_{1/2})$. To obtain a total $P(E_T)$ distribution for production of all 3-buten-1-yl radicals, we first normalize the $P(E_T)$'s for the production of each Br spin-orbit state shown in Fig. 14, then calculate the weighted sum of these $P(E_T)$'s which is equal to $0.833\times P(E_T)$ for producing $Br(^2P_{3/2})$ plus $0.167\times P(E_T)$ for producing $Br(^2P_{1/2})$. The $P(E_T)$ distribution thus obtained for all C–Br fission events producing the 3-buten-1-yl radicals is plotted in Fig. 16 with dashed line and the $P(E_T)$ for the same C–Br fission events producing 3-buten-1-yl radicals which are detected at $m/e=55$ with 157 nm photoionization is shown in solid line in Fig. 16. Clearly the high-recoil-kinetic-energy dissociation events produce low internal energy 3-buten-1-yl radicals which are not efficiently detected with 157 nm photoionization.

We now consider why photoionization at 157 nm might be able to detect high-internal-energy 3-buten-1-yl radicals, but not low-internal-energy radicals. First, note, as shown in Fig. 1, that 3-buten-1-yl radical could undergo ring closing and isomerization to form cyclopropylmethyl radical via a transition barrier of 12.3 kcal/mol as well as 2-1 hydrogen shift to form 1-methylallyl radical via a transition barrier of 32.2 kcal/mol. The 3-buten-1-yl radicals could also undergo H elimination to form $H+C_4H_6$. Among the isomerization and dissociation barriers, the hydrogen elimination (barrier of ~29.3 kcal/mol) and the isomerization to form 1-methylallyl radical are two possible steps which govern the reactivity of 3-buten-1-yl radical on the potential energy surface. Thus, one would expect that 3-buten-1-yl radicals formed with vibrational energy more than ~29 kcal/mol should be unstable to dissociation to form $H+1,3\text{-}C_4H_6$. Nevertheless, the low-kinetic-energy/high-internal-energy side of the $P(E_T)$ derived from detecting the radicals with photoionization at 157 nm matches the $P(E_T)$ derived from the momentum-matched bromine atoms fairly well. Note, however, that recoil kinetic energies of 17 kcal/mol leave the radical with 37.5 kcal/mol of internal energy if they are formed in conjunction with spin-orbit ground state bromine but only 27 kcal/mol if they are formed in conjunction with spin-orbit excited bromine atoms. Thus it is likely that many of the radicals detected in the low kinetic energy part of the distribution are formed in conjunction with spin-orbit excited state Br atoms. Near the threshold, some of the radicals formed in conjunction with spin-orbit ground state bromine may not be lost to dissociation by virtue of the energy imparted to rotation during the C–Br bond fission. For example, when 22 kcal/mol is partitioned to product translation in the photodissociation of the *trans*-precursor, an impulsive dissociation from the ground state equilibrium geometry predicts that 12.7 kcal/mol of the total internal energy of 32.5 kcal/mol is partitioned into rotational energy, leaving the radical with 19.8 kcal/mol, too little to surmount the barrier to C–H fission. These two effects explain why the low kinetic energy side of the $P(E_T)$ detected from photoionizing the stable radicals corresponds fairly closely with that derived from the momentum-matched Br atoms.

We now turn to the high-kinetic-energy side of the $P(E_T)$. Clearly starting at recoil kinetic energies near about 23 kcal/mol and continuing to the highest recoil kinetic energies of near 35 kcal/mol, the momentum-matched Br atoms evidence that 3-buten-1-yl radicals are being formed in the photodissociation events but the 157 nm photoionization is not detecting those radicals. At these recoil kinetic energies, the 3-buten-1-yl radicals are left with the lowest internal energies, a substantial amount of which is partitioned to rotation rather than vibration. For instance, at a recoil kinetic energy of 30 kcal/mol, where the Br signal is strong but very few radicals are detected, the internal energy of the radical is 24.5 kcal/mol but an impulsive dissociation predicts that 9.6 kcal/mol must be partitioned to rotation of the radical, leaving it with only 14.9 kcal/mol of internal vibrational energy. This gives us the information necessary to look for an explanation. In the high-recoil-kinetic-energy portion of this distribution, the radicals do not partition enough internal vibrational energy to allow them to surmount the 12.3 kcal/mol barrier to isomerization to form cyclopropylmethyl radicals. If the photoionization cross section of cyclopropylmethyl radicals was quite substantially higher than that of 3-buten-1-yl radicals at 157 nm, then we would preferentially detect radicals that could isomerize to cyclopropylmethyl but not those with too little vibrational energy to surmount that barrier. At energies above the isomerization barrier the equilibrium between the 3-buten-1-yl and cyclopropylmethyl forms favors the 3-buten-1-yl isomeric form, so the difference in photoionization probabilities would have to be quite substantial to support this explanation for why photoionization at 157 nm preferentially detects only 3-buten-1-yl radicals that can isomerize to cyclopropylmethyl radicals. We consider this proposal in light of electronic structure calculations presented below.

Our electronic structure calculations at the coupled cluster level of theory show that the 3-buten-1-yl radical is a stable radical as shown in Fig. 1 but it does not have a local

minimum in its cationic form. We have tried to locate the cationic structure of 3-buten-1-yl using the optimized geometry of the neutral radical as an initial structure; we found that the 3-buten-1-yl cation ($CH_2{=}{=}CHCH_2CH_2^+$) readily converts into 1-methylallyl cation ($CH_2CHCHCH_3^+$) by a 2,1 hydrogen shift. The 3-buten-1-yl cation is not a local minimum on the $C_4H_7^+$ potential energy surface and its instability could be understood by the fact that the positive charge and pi electrons are localized separately on both ends of the cation. While the 1-methylallyl cation has enhanced stability due to the resonance effect between the positive charge and the pi electrons (there are two possible resonance structures for 1-methylallyl cation), there is no similar stability effect from the pi electrons to the positive charge in the 3-buten-1-yl cation. Thus, upon photoionization the 3-buten-1-yl cation would undergo a barrierless 2,1-hydrogen shift to form the 1-methylallyl cation.

Table II gives the adiabatic and vertical IEs for the 1-methylallyl and 3-buten-1-yl radicals. The vertical IE is calculated as the energy difference (without correcting for zero-point energy difference) between the neutral and cation and the calculations are based on the optimized geometry of the neutral. The adiabatic IE for 3-buten-1-yl radicals forming 1-methylallyl cation (not the 3-buten-1-yl cation) is ~6.8 eV which is accessible by a 157 nm laser (7.90 eV), but we expect the Franck-Condon overlap for this adiabatic ionization to be very small. In contrast, the 1-methylallyl cation and cyclopropylmethyl cation are structurally similar to the neutral radicals. At photoionization energies above 8.5 eV one could expect to detect 3-buten-1-yl radicals via a near-vertical transition, though the cation would immediately isomerize on the $C_4H_7^+$ potential energy surface via a barrierless 2,1 hydrogen transfer to form 1-methylallyl cation. Thus, one can understand why nascent 3-buten-1-yl radicals formed with low vibrational energies are not efficiently detected in our experiments using 157 nm photoionization while higher internal energy radicals are. The higher internal energy radicals have sufficient internal vibrational energy (12.3 kcal/mol) to isomerize to the cyclopropylmethyl isomer, which can be efficiently photoionized at 157 nm, while the lower internal energy radicals are subject to a vertical IE which is much higher than the photoionization laser energy.

3. Photofragment angular distributions

Similar to our angular distribution analysis on 1-bromo-2-butene, we used Eqs. (5) and (6) to fit the angular distribution of the $Br(^2P_{1/2})$ and $Br(^2P_{3/2})$ fragments generated in the C–Br bond dissociation of 4-bromo-1-butene, respectively. Integrating the signal over the translational energy range of 15–30 kcal/mol for the $P(E_T)$ of $Br(^2P_{1/2})$ fragments gives an anisotropy parameter of 1.846±0.044 (the uncertainty is assigned based on the standard error from repeated measurements). The angular distribution fitting is displayed in Fig. 17(a) and the anisotropy parameter of ~1.85 indicates that most of the $Br(^2P_{1/2})$ fragments recoil in a direction parallel to the laser polarization. The anisotropy parameters for the angular distribution of the $Br(^2P_{3/2})$ are $\beta_2=0.908\pm0.015$ and $\beta_4=0.035\pm0.002$ with fits depicted in Fig. 17(b).

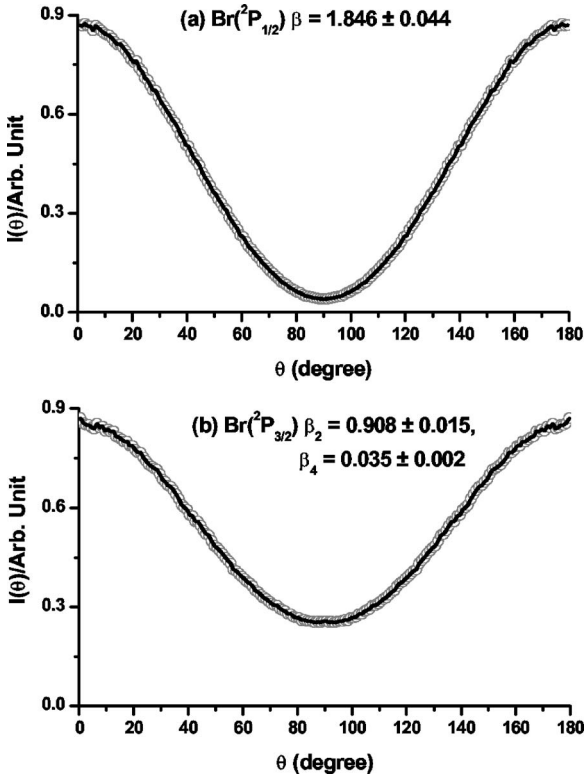

FIG. 17. Angular distribution fitting of (a) $Br(^2P_{1/2})$ and (b) $Br(^2P_{3/2})$ formed in the C–Br bond fission of 4-bromo-1-butene.

IV. DISCUSSION

We have studied the C–Br bond fission in the 234 nm photodissociation of 1-bromo-2-butene, 4-bromo-1-butene, and cyclopropylmethyl bromide. We have generated 1-methylallyl radicals by 234 nm C–Br bond fission of the 1-bromo-2-butene and photoionized the radical at 157 nm; by comparing the $P(E_T)$ of the 1-methylallyl radicals with the $P(E_T)$ measured from the momentum-matched Br cofragments, we have revised the relative REMPI line strength ratio for $Br(^2P_{3/2})$ (at 233.681 nm) to $Br(^2P_{1/2})$ (at 234.021 nm) to be 0.17±0.05. This revised REMPI line strength for $Br(^2P_{3/2})$ to $Br(^2P_{1/2})$ obtained from weighting the $P(E_T)$'s calculated from the Br atomic fragments in comparison with the $P(E_T)$ derived from kinetic energy measurements of the 1-methylallyl radical cofragments is slightly larger but still within the error range of the REMPI line strength of 0.10±0.07. The latter REMPI line strength, obtained from the same procedure with the Br and cyclobutyl fragments in the previous photodissociation study on cyclobutyl bromide, is likely to be less reliable because of the multiple photoionization channels of the cyclobutyl radicals accessible at photon energy of 7.9 eV and the insensitivity of the overall $P(E_T)$ fitting to the small branching from the $Br(^2P_{1/2})$ channels. The newly deduced REMPI ratio is supported by the fact that 1-methylallyl radical is generated with an internal energy ranged below its dissociation and isomerization barriers at 234 nm and it has a single photoionization channel (with very favorable Franck-Condon factor) accessible at 7.9 eV. Thus the assumption that the photoionization probability of the 1-methylallyl radicals is uniform over the

internal energies produced is very likely to be valid. Indeed, the newly deduced REMPI ratio gives a near perfect fit to the $P(E_T)$'s measured from the cyclopropylmethyl radicals and the momentum-matched Br cofragments which are produced in the 234 nm C–Br bond fission of cyclopropylmethyl bromide.

On the other hand, the comparison between the $P(E_T)$ derived from detecting the 3-buten-1-yl radicals and the total $P(E_T)$ from the kinetic energy measurement of the momentum-matched Br cofragments reveals that the low internal energy (high-recoil-kinetic-energy) 3-buten-1-yl radicals produced in the C–Br dissociation events are not efficiently detected with 157 nm photoionization. At recoil kinetic energies of 23 kcal/mol and above, the data suggest the 3-buten-1-yl radicals to have too little internal vibrational energy, due to partitioning of the internal energy into rotation to conserve angular momentum, to surmount the 12.3 kcal/mol barrier to isomerization to form cyclopropylmethyl radicals. Based on the theoretical prediction, the 3-buten-1-yl radicals would adiabatically ionize into the 1-methylallyl cation and the photoionization cross section of 3-buten-1-yl radicals at 157 nm is substantially lower than that of cyclopropylmethyl radicals; we preferentially detect radicals that could isomerize to cyclopropylmethyl but not those with too little vibrational energy to surmount that isomerization barrier. On the low-recoil-kinetic-energy, higher internal energy side of the spectrum, we expected to observe some loss of radicals to the 1,3-butadiene+H dissociation channel, but we were able to detect low recoil kinetic release 3-buten-1-yl radicals by the photoionization at 157 nm because those radicals (with high internal energy) have partitioned enough of the internal energy to rotation rather than vibration and this leaves the radical with an internal vibrational energy less than the barrier to dissociation to 1,3-butadiene+H but with enough internal energy to isomerize to the easily photoionized cyclopropylmethyl form.

Recently, Fan and Pratt[22] have observed that the hydrocarbon radicals such as C_2H_5, n-C_3H_7, and i-C_3H_7 have photoionization cross sections that are nearly constant with internal energy of the radicals. They prepared hydrocarbon radicals by photodissociating the corresponding iodoprecursor and measured the $P(E_T)$'s of both hydrocarbon radicals and iodine cofragments. Based on the comparison of the $P(E_T)$'s, they found that the relative photoionization cross section and the detection efficiency are almost independent of the internal energy of the nascent radicals generated. On the other hand, our present observation that the 3-buten-1-yl radicals formed in higher recoil kinetic energy C–Br fission events (those radicals have lower internal energies) are not efficiently detected by 157 nm photons while the radicals formed in lower recoil kinetic energy range are effectively photoionized is an important but easily understood counterexample to Fan and Pratt's findings. When the vertical IE of a neutral species is much higher than the photoionization energy, the species cannot be efficiently ionized, but if the neutral species has enough internal energy to isomerize to an isomer with a lower vertical IE (in our case, the 3-buten-1-yl radical could isomerize into cyclopropylmethyl radical with a lower IE value), then the internal energy dependence of the photoionization cross section can be quite dramatic as evidenced in our study of the 3-buten-1-yl radical.

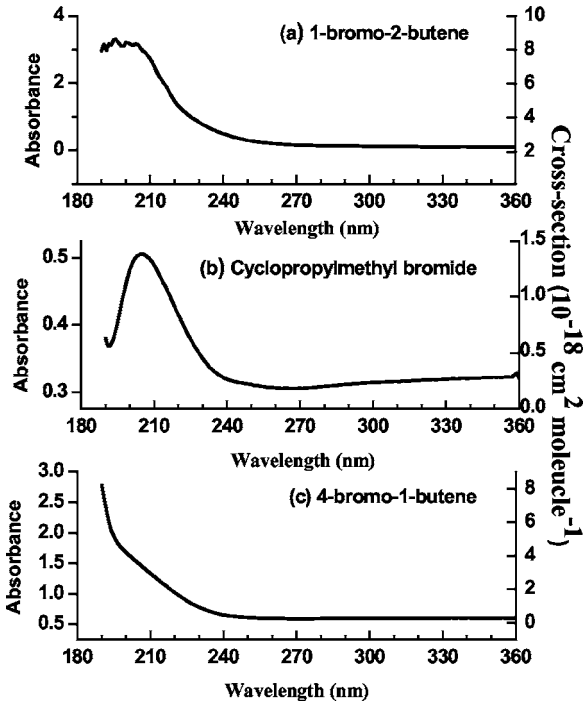

FIG. 18. Gas phase ultraviolet absorption spectrum of (a) 1-bromo-2-butene, (b) cyclopropylmethyl bromide, and (c) 4-bromo-1-butene.

Figure 18 shows the ultraviolet absorption spectrum of 1-bromo-2-butene, cyclopropylmethyl bromide, and 4-bromo-1-butene. The spatial anisotropy parameters β for Br($^2P_{1/2}$), Br($^2P_{3/2}$), and C_4H_7 data obtained in the present study are summarized in Table III. The absorption band of cyclopropylmethyl bromide is similar to that of methyl bromide but shifted to the red. Thus, we expect the 234 nm photon excites a nonbonding electron of Br to the σ^*(C–Br) orbital, promoting the molecule to potential energy surfaces of cyclopropylmethyl bromide which are repulsive along the C–Br bond. The uv photochemistry of methyl bromide is governed by the dissociative excited electronic states $^3Q_1$, $^3Q_0$, and $^1Q_1$. Among these states, only the $^3Q_0$ state correlates diabatically to the spin-orbit excited Br($^2P_{1/2}$) channel while the $^3Q_1$ and $^1Q_1$ states correlate diabatically to the ground state Br($^2P_{3/2}$) channel. Photoexcitation to the $^3Q_0$ state from the ground state corresponds to a parallel transition ($\beta=+2$) while the transitions to the $^3Q_1$ and $^1Q_1$ are perpendicular ($\beta=-1$) with transition dipole moment perpendicular to the C–Br bond. Both the Br($^2P_{3/2}$) and Br($^2P_{1/2}$) channels are mediated by the curve crossing interaction of the $^3Q_0$ and $^1Q_1$ states.

The spatial anisotropy parameter β value of 1.640 for Br($^2P_{1/2}$) is close to limiting value of +2; this indicates that the initially excited repulsive $n\sigma^*$(C–Br) state of cyclopropylmethyl bromide at 234 nm is accessed largely through a parallel transition and asymptotically dissociates into Br($^2P_{1/2}$) and cyclopropylmethyl fragments. This repulsive state is analogous to the $^3Q_0$ state of the CH_3Br molecule as mentioned above. The deviation of Br($^2P_{1/2}$) angular distri-

TABLE III. A summary of the anisotropy parameters for the $Br(^2P_{1/2})$ and $Br(^2P_{3/2})$ channels and the spin-orbit branching ratios obtained in this study.

	$Br(^2P_{1/2})$	$Br(^2P_{3/2})$	C_4H_7	$Br(^2P_{1/2}):Br(^2P_{3/2})$ spin-orbit branching
1-bromo-2-butene	$\beta=0.372\pm0.001$	$\beta_2=0.236\pm0.005$ $\beta_4=0.032\pm0.001$	$\beta=0.339\pm0.006$	67% : 33%
Cyclopropylmethyl bromide	$\beta=1.640\pm0.021$	$\beta_2=0.775\pm0.016$ $\beta_4=0.032\pm0.003$ $\beta=0.673\pm0.016$	$\beta=0.902\pm0.034$	18% : 82%
4-bromo-1-butene	$\beta=1.846\pm0.044$	$\beta_2=0.908\pm0.015$ $\beta_4=0.035\pm0.002$ $\beta=0.816\pm0.015$	···	17% : 83%

bution from pure parallel transition may result from several reasons. First, photoexcitation of cyclopropylmethyl bromide at 234 nm may involve a small overlapping absorption to the excited states analogous to the $^3Q_1$ state or the $^1Q_1$ states of the CH_3Br molecule accessed by perpendicular transition. Nonadiabatic curve crossing from the $^1Q_1$ diabat to the $^3Q_0$ diabat analog in cyclopropylmethyl bromide may proceed along the C–Br bond stretching coordinate and produce $Br(^2P_{1/2})$ fragments adiabatically, thus contributing some perpendicular character to the $Br(^2P_{1/2})$ fragment angular distribution. In addition, the vibrational bending motion in the excited parent molecule will also decrease the dissociation product recoil anisotropy. Likewise, the $Br(^2P_{3/2})$ atoms may also be produced from dissociation on the $^3Q_1$ state or the $^1Q_1$ states diabatically and via the curve crossing, avoided at nonsymmetric geometries, between the $^3Q_0$ and the $^1Q_1$ states. Indeed, the measured anisotropy parameter of 0.673 for $Br(^2P_{3/2})$, having a parallel character, but more perpendicular character than that of the $Br(^2P_{1/2})$ fragment, indicates that absorption to the $^3Q_1$ state may play a role. The anisotropic angular distribution of cyclopropylmethyl bromide is very similar to that of cyclobutyl bromide observed in our previous study.[14]

The spatial anisotropy parameters for the $Br(^2P_{1/2})$ and $Br(^2P_{3/2})$ channels of 4-bromo-1-butene are similar to that of the cyclopropylmethyl bromide. As shown in the Fig. 18, the uv absorption of 4-bromo-1-butene is blue-shifted relative to that of cyclopropylmethyl bromide. The anisotropy parameters for the $Br(^2P_{1/2})$ channel of the 4-bromo-1-butene are expected to be more parallel because there should have less contribution from the higher energy $^1Q_1$ state. This expectation is confirmed by the larger β value of 1.846 for the $Br(^2P_{1/2})$ production channel of 4-bromo-1-butene.

The 1-bromo-2-butene has noticeably different angular distributions at 234 nm compared with other two hydrocarbon bromides in this study. The spatial anisotropy parameters of 1-bromo-2-butene for $Br(^2P_{1/2})$ channel is considerably smaller than those of the cyclobutyl and cyclopropylmethyl bromides. We expect the 234 nm photon excites a nonbonding electron of Br to the $n\sigma^*$(C–Br) orbital, promoting the molecule to a repulsive potential energy surfaces of 1-bromo-2-butene along the C–Br bond, but there may be considerable configuration interaction with the $\pi\pi^*$ excited configuration of the nearby C=C bond. The value of $\beta=0.372\pm0.001$ observed in the $Br(^2P_{1/2})$ channel might not be correctly interpreted by suggesting that the perpendicular transition from ground state to $^1Q_1$ state makes a significant contribution to the production of $Br(^2P_{1/2})$ atomic fragments through the avoided curve crossing between the $^3Q_0$ and the $^1Q_1$ states. The increased contribution of this perpendicular transition may be attributed to the intensity borrowing from the nearby singlet $\pi\rightarrow\pi^*$ transition of the C=C bond. The present anisotropic angular distribution of 1-bromo-2-butene bromide is similar to that of allyl bromide observed by Park *et al.*[10]

In the 234 nm C–Br dissociation of 1-bromo-2-butene, 67% of the C–Br bond fission events produce $Br(^2P_{1/2})$ and ~33% of the C–Br fission events produce $Br(^2P_{3/2})$: this results in a $Br(^2P_{1/2})$ to $Br(^2P_{3/2})$ product branching ratio of 2.03:1. The respective $Br(^2P_{1/2})$ to $Br(^2P_{3/2})$ product branching ratios are 0.22:1 and 0.20:1 in the 234 nm C–Br dissociation of cyclopropylmethyl bromide and 4-bromo-1-butene; this means ~17% of the C–Br bond fission events produce $Br(^2P_{1/2})$ and ~83% of the C–Br fission events produce $Br(^2P_{3/2})$ for both molecules. The internal energy distributions of the nascent radicals are plotted on the potential energy surface of the C_4H_7 radicals in Fig. 19; the distributions are constructed by weighted sum of the individual $P(E_T)$'s of $Br(^2P_{1/2})$ and $Br(^2P_{3/2})$ with the newly derived REMPI line strength factor (note that the channel producing excited spin-orbit Br fragments has 10.54 kcal/mol less available energy after 234 nm photodissociation). Both the cyclopropylmethyl and 3-buten-1-yl radicals have internal energy distributions that spanned over the isomerization and/or dissociation barriers, but we are able to detect those radicals (see Secs. III B 1 and III D 1) because part of the internal energies of these radicals has been partitioned into rotational motion and this leaves the radicals with insufficient internal vibrational energy to surmount the barriers. The internal energy distribution of the cyclobutyl radicals is included for completeness: this distribution has been constructed using the newly deduced REMPI line strength ratio. In this study, we have shown that the 234 nm C–Br bond fissions of 1-bromo-2-butene, 4-bromo-1-butene, and cyclopropylmethyl bromide serves as potential photolytic precursors that generate the corresponding 1-methylallyl,

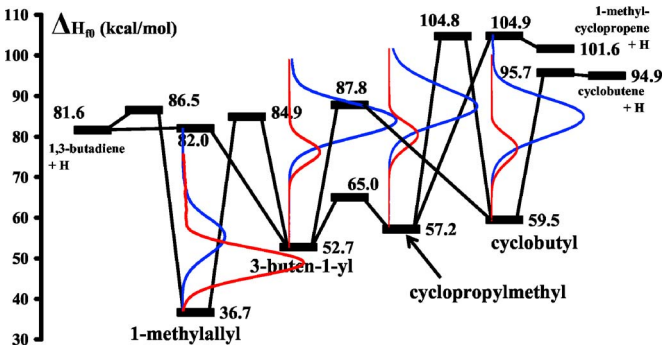

FIG. 19. (Color online) Potential energy surface displaying energetics for the dissociation and isomerization channels among the 1-methylallyl, cyclopropylmethyl, 3-buten-1-yl, and cyclobutyl radicals from Fig. 1. The internal energy distributions of the nascent radicals generated in this study are shown by the overlaid curve above the corresponding radicals. Note that the internal energy distribution of the radical are determined from momentum conservation with the detected Br fragments and energy conservation, correcting for the fact that the radicals produced in coincidence with $Br(^2P_{1/2})$ have 10.54 kcal/mol less internal energy. The contribution shown in red in the online version corresponds to the internal energy distribution of C_4H_7 radicals formed with the $Br(^2P_{1/2})$ cofragments and contribution shown in blue in the online version represents the internal energy distribution of C_4H_7 radicals formed with the $Br(^2P_{3/2})$ cofragments.

3-buten-1-yl, and cyclopropylmethyl radicals. Based on the $P(E_T)$ measurements of the momentum-matched Br atomic fragments, we do not observe any excited radicals but only the ground state of these radicals formed in the 234 nm C–Br bond fission.

V. CONCLUSIONS

The 234 nm C–Br photolytic bond cleavages of 1-bromo-2-butene, 4-bromo-1-butene, and cyclopropylmethyl bromide have been studied using velocity map imaging method. We have used 2+1 state-selective REMPI to probe the $Br(^2P_{3/2})$ and $Br(^2P_{1/2})$ fragments and 157 nm photons to ionize the C_4H_7 cofragments. Based on conservation of energy and momentum, the internal energy distributions of the nascent momentum-matched radicals are derived. In the case of the 1-methylallyl radical the photoionization cross section is expected to be independent of internal energy in the range of 7–30 kcal/mol. Thus, by comparing between the $P(E_T)$ derived from the measurement of the 1-methylallyl velocity distribution and the $P(E_T)$ obtained from a weighted sum of individual $P(E_T)$'s of the Br fragments to match the former distribution, we have deduced a product branching radio and a new REMPI line strength ratio for $Br(^2P_{3/2})$ and $Br(^2P_{1/2})$ at 233.681 and 234.021 nm, respectively. This new REMPI line strength is 0.17 ± 0.05 and compares favorably with the line strength ratio of 0.10 ± 0.07 which was determined using a similar procedure in the previous 234 nm photodissociation of cyclobutyl bromide. The present study suggests that the photoionization cross section does not strongly depend on the internal energy of the radical. The new line strength ratio has also been used to determine the branching of the $Br(^2P_{3/2})$ and $Br(^2P_{1/2})$ product channels for cyclopropylmethyl bromide and 4-bromo-1-butene and to determine the internal energy distribution of their momentum-matched radicals. We find that 157 nm photoionization of cyclopropylmethyl radicals is relatively insensitive to internal energy, while 3-buten-1-yl radicals show a photoionization cross section that is markedly dependent on internal energy with the lowest internal energy radicals not efficiently detected by photoionization at 157 nm. We have carried out electronic structure calculations of the radicals and their cations to interpret the experimental results. The spatial angular distribution and photodissociation dynamics of all three molecular systems have been discussed as well.

ACKNOWLEDGMENT

This work was supported by the National Science Foundation under Grant No. CHE-0403471 (L.J.B.).

[1] J. L. Miller, M. J. Krisch, L. J. Butler, and J. N. Shu, J. Phys. Chem. A **109**, 4038 (2005).
[2] L. R. McCunn, M. J. Krisch, Y. Liu, L. J. Butler, and J. N. Shu, J. Phys. Chem. A **109**, 6430 (2005).
[3] L. R. McCunn, K. C. Lau, M. J. Krisch, L. J. Butler, J. W. Tsung, and J. J. Lin, J. Phys. Chem. A **110**, 1625 (2006).
[4] L. Koziol, S. V. Levchenko, and A. I. Krylov, J. Phys. Chem. A **110**, 2746 (2006).
[5] W. McNavage, M. Wilhelm, R. Groller, and H. L. Dai, Abstr. Pap. - Am. Chem. Soc. **228**, U224 (2004).
[6] J. D. DeSain, L. E. Jusinski, and C. A. Taatjes, Phys. Chem. Chem. Phys. **8**, 2240 (2006).
[7] T. Gougousi, P. C. Samartzis, and T. N. Kitsopoulos, J. Chem. Phys. **108**, 5742 (1998).
[8] R. S. Zhu, B. F. Tang, L. Ji, Y. Tang, S. Zhang, and B. Zhang, J. Opt. Commun. **235**, 325 (2004).
[9] M. L. Morton, J. L. Miller, L. J. Butler, and F. Qi, J. Phys. Chem. A **106**, 10831 (2002).
[10] M. S. Park, K. W. Lee, and K. H. Jung, J. Chem. Phys. **114**, 10368 (2001).
[11] J. C. Schultz, F. A. Houle, and J. L. Beauchamp, J. Am. Chem. Soc. **106**, 7336 (1984).
[12] K. C. Lau, Y. Liu, and L. J. Butler, J. Chem. Phys. **123**, 054322 (2005).
[13] Y. Liu and L. J. Butler, J. Chem. Phys. **121**, 11016 (2004).
[14] Y. Liu, K. C. Lau, and L. J. Butler, J. Phys. Chem. A **110**, 5379 (2006).
[15] V. Dribinski, A. Ossadtchi, V. A. Mandelshtam, and H. Reisler, Rev. Sci. Instrum. **73**, 2634 (2002).
[16] A. G. Baboul, L. A. Curtiss, P. C. Redfern, and K. Raghavachari, J. Chem. Phys. **110**, 7650 (1999).
[17] L. A. Curtiss, P. C. Redfern, V. Rassolov, G. Kedziora, and J. A. Pople, J. Chem. Phys. **114**, 9287 (2001).
[18] T. P. Rakitzis and R. N. Zare, J. Chem. Phys. **110**, 3341 (1999).
[19] T. P. Rakitzis, S. A. Kandel, A. J. Alexander, Z. H. Kim, and R. N. Zare, J. Chem. Phys. **110**, 3351 (1999).
[20] P. C. Samartzis, B. L. G. Bakker, T. P. Rakitzis, D. H. Parker, and T. N. Kitsopoulos, Chem. Phys. Lett. **110**, 5201 (1999).
[21] T. P. Rakitzis, Chem. Phys. Lett. **342**, 121 (2001).
[22] H. Y. Fan and S. T. Pratt, J. Chem. Phys. **123**, 204301 (2005).